Performance Analysis for Multihop Full-Duplex IoT Networks Subject to Poisson Distributed Interferers

Gaojie Chen, *Senior Member, IEEE*, Justin P. Coon, *Senior Member, IEEE*, Avishek Mondal, Ben Allen, *Senior Member, IEEE*, and Jonathon A. Chambers, *Fellow, IEEE*

***Abstract*—Multihop relaying is a fundamental technology that will enable connectivity in large-scale networks such as those encounted in Internet of Things applications. However, the end-to-end transmission rate decreases dramatically as the number of hops increases when half-duplex (HD) relaying is employed. In this paper, we investigate the outage probability and symbol-error rate for both HD and full-duplex (FD) transmission schemes in multihop networks subject to interference from randomly distributed third-party devices. We model the locations of the interfering devices as a Poisson point process. We derive a closed-form expression for the outage probability and approximations for the symbol-error rate for HD and FD transmissions employing BPSK and QPSK. The symbol-error rate results are obtained by using a Markov chain model for the multihop decode-and-forward links. This model accurately accounts for the nonlinear dynamical nature of the network, whereby erroneous symbol decoding can be "corrected" by a second erroneous decoding operation later in the network. We verify the analytical results through simulations and show the HD and FD schemes can be utilized to reduce the error-rate and outage probability of the system according to different residual self-interference levels and interferer densities. The results provide clear guidelines for implementing HD and FD in multihop networks.**

***Index Terms*—Full-duplex (FD), multihop networks, performance analysis, stochastic geometry.**

I. Introduction

THE emerging requirements of network ubiquity and machine intelligence that are needed to support and enhance future economic and social development have led to the Internet of Things (IoT) vision and have accelerated a number technological advances in recent years [1]. Unlike traditional mobile computing scenarios, the IoT is evolving into an ecosystem that facilitates the connection of physical objects (e.g., sensors and actuators) augmented by embedded intelligence [2]–[4].

To realize the IoT vision, a large number of heterogeneous devices must continuously generate sensing data and communicate this data across the network. At present, Long Term Evolution-Advanced (LTE-A) is utilized for the communication task. However, the original target of LTE-A was to provide high data rates using large data packets. For IoT applications that use small data packets, LTE-A can be an inefficient means of communicating. To make matters worse, the typically high energy consumption required by LTE-A is a severe obstacle to large-scale IoT deployments via cellular connectivity [1]. Consequently, novel solutions are required to enable the efficient use of radio resources to convey the small data packets typically exchanged by IoT applications in large-scale networks.

Multihop relaying offers a promising solution that is capable of reducing energy consumption and extending the coverage of wireless networks. For example, multihop transmission is beneficial for ensuring the quality-of-service of remote nodes is achieved without increasing the transmit power [5]. Moreover, multihop relay systems have been utilized widely in device-to-device and machine-to-machine communications where the number of wireless devices that can potentially serve as intermediate relaying nodes is large [6]–[8]. With the development of millimeter-wave communications, multihop transmission will be implemented at high frequencies to avoid interference between two transmitters [9].

Conventionally, multihop relay systems operate in half-duplex (HD) mode that uses either multiple time slots or orthogonal frequencies for signal transmission and reception. With the number of hops increasing, however, required number of time slots or frequency bands for packet forwarding increases significantly. To overcome this problem, one may turn to full-duplex (FD) transmission. Thanks to the enormous progress made in the development of self-interference (SI) cancellation techniques [10], [11], FD multihop communication is now possible.

Multihop FD networks have recently been studied in [12]–[15]. Ju *et al.* [12] provided throughput and delay analyses of beamforming-based FD transmission. Wu *et al.* [13] formulated optimization problems for the transceiver filter design and power allocation in a multihop decode-and-forward (DF) FD relay system with imperfect channel state information (CSI). The power allocation problem was solved using geometric programming and an alternating

Manuscript received August 28, 2018; revised November 1, 2018; accepted November 30, 2018. Date of publication December 7, 2018; date of current version May 8, 2019. This work was supported in part by EPSRC Grant EP/R006377/1 ("M3NETs") and Grant EP/N002350/1 ("Spatially Embedded Networks") and in part by the Royal Society Industry Fellowship Scheme under Grant IF160001. *(Corresponding author: Gaojie Chen.)*

G. Chen and J. A. Chambers are with the Department of Engineering, University of Leicester, Leicester LE1 7RH, U.K. (e-mail: gaojie.chen@leicester.ac.uk; jonathon.chambers@leicester.ac.uk).

J. P. Coon and A. Mondal are with the Department of Engineering Science, University of Oxford, Oxford OX1 3PJ, U.K. (e-mail: justin.coon@eng.ox.ac.uk).

B. Allen is with the Department of Engineering Science, University of Oxford, Oxford OX1 3PJ, U.K., and also with Network Rail, London NW1 2DN, U.K. (e-mail: ben.allen@eng.ox.ac.uk).

Digital Object Identifier 10.1109/JIOT.2018.2885756

optimization approach. Baranwal *et al.* [14] analyzed and compared the performance of FD and HD systems in a multihop relay system. To provide a more practical system, an unsaturated FD multihop scheme is investigated in [15] by using power allocation technique.

Interference has not, however, been examined in all of the above papers, which does not present a realistic scenario when considering dense networks. For example, for IoT and massive machine-type communications, the interference from other active nodes should be considered when analyzing system performance [16]. To address this issue, we will utilize stochastic geometry [17] to derive a practical and tractable analytic framework for FD multihop DF networks subject to interference from other active nodes. We assume that the locations of interfering nodes are modeled as a homogeneous poisson point process (PPP). To the best of the authors' knowledge, this is the first work to exploit a Markov chain model to investigate the symbol-error rate (SER) and outage probability in FD multihop DF networks in the presence of randomly located interferers. The contributions of this paper are the following.

1) We derive exact and approximate expressions for the end-to-end outage probability and SER for HD and FD multihop DF relay networks by using a Markov chain model. BPSK and QPSK are explicitly considered for the SER analysis, and a general framework is described for analyzing other modulation schemes.
2) We conduct an asymptotic performance analysis in order to gain insight into system behavior for two regimes: a) interference-limited networks and b) noise-limited networks.
3) We provide extensive simulations and numerical results to verify the theoretical analysis.

The remainder of this paper is organized as follows. In Section II, the system model and problem formulation are described. In Section III, an analysis of the outage probability for HD and FD transmission schemes is detailed. A derivation of the SER for the HD and FD scenarios considering BPSK and QPSK is given in Section IV. Section V contains details of the asymptotic performance analysis. Section VI provides numerical simulations that verify the analysis. Section VII gives a summary of this paper.

II. System Model and Problem Formulation

We study a multihop FD network operating in the presence of randomly located interferers as shown in Fig. 1, where the transmitter (S_0) transmits the information to the destination (S_N) by using a number of DF relays (S_i, $i \in (1, 2, \ldots, N-1)$). We assume the transmitter, all of the relay nodes and the destination are located at the origin and fixed locations away from the origin, respectively, in a 2-D plane. We also assume that the locations of the interferers are modeled by using a homogeneous PPP, Φ_I, which has density ρ_I. To be specific, the source and destination devices are equipped with HD antennas so that they do not transmit and receive simultaneously; the relays are equipped with a hyper-duplex antenna which

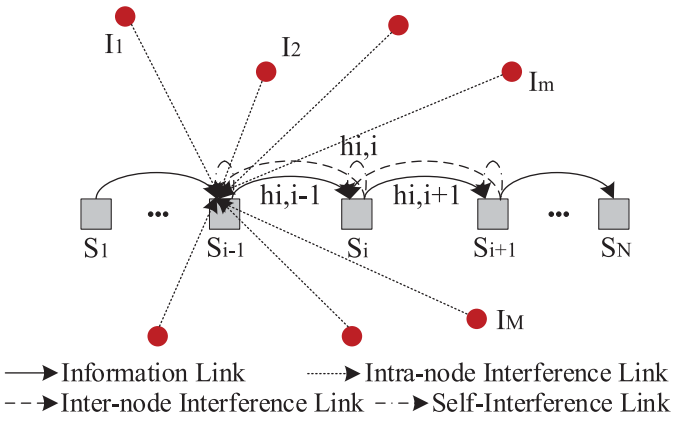

Fig. 1. Wireless network with randomly located EDs.

can easily switch between the HD and FD modes according to system needs. All channels are assumed to experience path loss and independent Rayleigh fading effects modeled as $h_{ij} = \mu_{ij} d_{ij}^{-\alpha/2}$, where α and d_{ij} denote the path loss exponent and the distance between two nodes, i and j, respectively. The fading coefficient μ_{ij} is a complex Gaussian random variable with unit variance. Therefore, the corresponding channel gain $|h_{ij}|^2$ is independently, exponentially distributed with mean $\lambda_{ij} = \mathbb{E}[|h_{ij}|^2] = d_{ij}^{-\alpha}$. The noise variances are normalized to one, and the channels are assumed to be quasi-static so that the channel coefficients remain unchanged during each transmission block but vary independently from one block to another.

We assume that the CSI between two adjacent nodes is known by the receiving node.[1] Therefore, for the FD scenario, S_{i-1} can send a symbol x_{i-1} to S_i. At the same time, S_i receives the relay interference,[2] SI, and third-party interference from S_{i+1}, itself, and active third-party interference, respectively. Hence, the received signal at S_i can be written as

$$y_i = \frac{\sqrt{P_{T_{i-1}}} h_{i-1,i}}{d_{i-1,i}^{\frac{\alpha}{2}}} x_{i-1} + \sum_{m \in \Phi_I} \frac{\sqrt{P_{I_m}} h_{m,i}}{d_{m,i}^{\frac{\alpha}{2}}} x_m + \sqrt{P_{T_i}} h_{i,i} x_i + \frac{\sqrt{P_{T_{i+1}}} h_{i+1,i}}{d_{i+1,i}^{\frac{\alpha}{2}}} x_{i+1} + n_i \quad (1)$$

where P_{T_i} denotes the transmit power of the ith node, P_{I_m} denotes the transmit power of the mth intrainterferer, and n_i denotes additive white Gaussian noise with unit power. For simplicity, we assume that $P_{T_i} = P_T$ for $i \in \{0, 1, \ldots, N-1\}$ and $P_{I_m} = P_I$ for $m \in \Phi_I$.[3] The second term of (1) denotes the interference from the third-party interferers; the third and fourth terms of (1) denote the SI and relay interference, respectively. Note that there is no SI and relay interference in HD

[1]The CSI is usually estimated through pilots and feedback, e.g., [18]. CSI estimation without feedback may also be applied, e.g., [19]. Further detail of CSI estimation is beyond the scope of this paper.

[2]The relay interference occurs mainly from relay nodes that are one hop away rather than relay nodes two hops away or more, which is a similar assumption made in two-hop networks without the direct link [20]–[22].

[3]P_T and P_I are equivalent to the transmit power to noise power ratio and the interference power to noise ratio in dB, respectively, because the noise power has been normalized to unity in this paper.

relay networks. Furthermore, for FD relays, SI and relay interference can be mitigated by using an SI cancellation scheme[4] and a network coding cancellation scheme.[5] Therefore, the signal-to-noise-plus-interference ratio at the S_i for HD and FD relays can be written as

$$\gamma_{S_i}^{\mathrm{HD}} = \frac{\frac{P_T|h_{i-1,i}|^2}{d_{i-1,i}^{\alpha}}}{\sum_{m\in\Phi_I}\frac{P_I|h_{m,i}|^2}{d_{m,i}^{\alpha}}+1} \tag{2}$$

$$\gamma_{S_i}^{\mathrm{FD}} = \frac{\frac{P_T|h_{i-1,i}|^2}{d_{i-1,i}^{\alpha}}}{\sum_{m\in\Phi_I}\frac{P_I|h_{m,i}|^2}{d_{m,i}^{\alpha}}+\gamma_{i,i}+1} \tag{3}$$

where $\gamma_{i,i}$ denotes the residual SI channel gain.[6]

III. Outage Probability Analysis

Here, we investigate the outage probability of HD and FD multihop networks. First, by using the following lemma, the cumulative distribution function (CDF) of γ_{S_i} for both the HD and the FD cases can be obtained.

Lemma 1: The CDF of γ_{S_i} for the HD and FD scenarios are given by

$$F_{\gamma_{S_i}}^{\mathrm{HD}}(z) = 1-\exp\left(-\frac{zd_{i-1,i}^{\alpha}}{P_T}\right)\exp\left(-z^{\frac{2}{\alpha}}\Omega_i\right) \tag{4}$$

$$F_{\gamma_{S_i}}^{\mathrm{FD}}(z) = 1-\frac{P_T e^{-\frac{zd_{i-1,i}^{\alpha}}{P_T}}}{d_{i-1,i}^{\alpha}\lambda_{ii}z+P_T}\exp\left(-z^{\frac{2}{\alpha}}\Omega_i\right) \tag{5}$$

where λ_{ii} denotes the average residual SI channel gain and

$$\Omega_i = \frac{\pi d_{i-1,i}^2\rho_M P_I^{\frac{2}{\alpha}}}{P_T^{\frac{2}{\alpha}}\mathrm{sinc}\left(\frac{2}{\alpha}\right)}.$$

Proof: See Appendix A. ∎

Remark 1: For given $d_{i,i+1}$, the outage probability between any two nodes for the HD case depends on the intensity of the interferer process, the path loss exponent α, and the transmit powers P_T and P_I. For the FD case, except for the above parameters, the outage probability is affected by residual SI as well.

The probability density function (PDF) of γ_{S_i} for the HD and FD cases can be written as

$$f_{\gamma_{S_i}}^{\mathrm{HD}}(z) = \left(\frac{2\Omega_i}{\alpha}z^{\frac{2}{\alpha}-1}+\frac{d_{i-1,i}^{\alpha}}{P_T}\right)\exp\left(-\frac{zd_{i-1,i}^{\alpha}}{P_T}-z^{\frac{2}{\alpha}}\Omega_i\right) \tag{6}$$

and (7), shown at the bottom of the next page, respectively. Since DF relays have been utilized to forward information signal from the source to the destination, by using (4) and (5), the end-to-end outage probability for HD and FD systems can be written as

$$P_o^{\Xi}(z) = 1-\prod_{i\in\{1,\ldots,N\}}\left(1-F_{\gamma_{S_i}}^{\Xi}(z)\right) \tag{8}$$

where $\Xi\in\{\mathrm{HD},\mathrm{FD}\}$, $z=2^{NR_s}-1$ for the HD case, $z=2^{(N+1)R_s/N}-1$ for the FD case, and R_s is the target rate.

IV. Error Probability Analysis

Although outage probability is easy to compute and gives some insight into the theoretical end-to-end performance of a multihop network, it is often more desirable in practice to characterize the SER for a chosen modulation scheme. Hence, in this section, we are interested in calculating the end-to-end probability that a symbol is decoded in error. We invoke a Markov chain model of the relay network to analyze the error probability. This is a useful model since it takes into consideration errors induced by the channel at one part of the system that may be corrected through a further fortunate error later in the network.

A. Case Study for BPSK

For BPSK, the symbol error probability conditioned on the SNR (γ_{S_i}) at the ith hop is given as

$$p_{i|\gamma_{S_i}} = \frac{1}{2}\,\mathrm{erfc}\left(\sqrt{\gamma_{S_i}}\right) \tag{9}$$

where $\mathrm{erfc}(x)$ denotes the complementary error function. Thus, we have expressions for the SER for each hop based on γ_{S_i}, and the following transition matrix for the ith hop can be constructed:

$$\mathbf{P}_{i|\gamma_{S_i}} = \begin{pmatrix} 1-p_{i|\gamma_{S_i}} & p_{i|\gamma_{S_i}} \\ p_{i|\gamma_{S_i}} & 1-p_{i|\gamma_{S_i}} \end{pmatrix}. \tag{10}$$

In general, if the prior distribution of the transmitted symbol is given by the vector $\mathbf{p}_0=(\epsilon,1-\epsilon)^T$, where $\epsilon=\mathbb{P}(X=-\sqrt{P_T})$ and $1-\epsilon=\mathbb{P}(X=\sqrt{P_T})$, then the posterior distribution of decoded symbols at the nth receiver (i.e., after n hops) is

$$\mathbf{p}_n = \mathbf{P}_{n|\gamma_{S_n}}\cdots\mathbf{P}_{1|\gamma_{S_1}}\mathbf{p}_0 = \prod_{i=1}^{n}\mathbf{P}_{i|\gamma_{S_i}}\mathbf{p}_0. \tag{11}$$

The probability that a symbol is decoded erroneously at the nth receiver is

$$P_{s|\gamma_{S_i}} = \epsilon\mathbb{P}\left(\overline{+}|+\right)+(1-\epsilon)\mathbb{P}\left(\overline{-}|-\right) \tag{12}$$

where $\overline{A}$ denotes the decoding result, which is not A when A is transmitted. The first conditional probability of error after n hops can be written as

$$\mathbb{P}\left(\overline{+}|+\right) = 1-\mathbf{u}_1^T\mathbf{P}_{n|\gamma_{S_n}}\cdots\mathbf{P}_{1|\gamma_{S_1}}\mathbf{u}_1 \tag{13}$$

where $\mathbf{u}_j$ is the jth column of the 2×2 identity matrix. $\mathbb{P}(\overline{-}|-)$ can be written similarly. $\mathbf{P}_{i|\gamma_{S_i}}$ is a symmetric matrix, and can thus be decomposed easily. The eigenvalues are

[4]The details of SI cancellation for FD implementation is beyond the scope of this paper. More related details can be found in [11] and references therein.

[5]The CSI between two neighbor nodes can be obtained, therefore, physical layer network coding cancellation [23] can be applied to completely mitigate the relay interference.

[6]According to [24], radio transmissions always encounter a bandwidth constraint so that SI cannot always be cancelled completely. Therefore, it is essential to define the residual SI channel gain $\gamma_{i,i}$.

$\lambda = 1, 1-2p_{i|\gamma_{S_i}}$ and the corresponding normalized eigenvectors are

$$\mathbf{v}_1 = \left(\frac{1}{\sqrt{2}}, \frac{1}{\sqrt{2}}\right)^T \text{ and } \mathbf{v}_2 = \left(\frac{1}{\sqrt{2}}, -\frac{1}{\sqrt{2}}\right)^T. \quad (14)$$

Hence, we can rewrite the expression given above as

$$\mathbb{P}(\overline{+}|+) = 1 - \mathbf{u}_1^T \mathbf{V} \mathbf{\Lambda}_n \cdots \mathbf{\Lambda}_1 \mathbf{V}^T \mathbf{u}_1 \quad (15)$$

where $\mathbf{\Lambda}_i = \text{diag}\{1, 1-2p_{i|\gamma_{S_i}}\}$ and $\mathbf{V} = [\mathbf{v}_1 \ \mathbf{v}_2]$. Now, we have

$$\mathbb{P}(\overline{+}|+) = \mathbb{P}(\overline{-}|-) = \frac{1}{2} - \frac{1}{2}\prod_{i=1}^{n}\left(1-2p_{i|\gamma_{S_i}}\right). \quad (16)$$

Thus, for $\epsilon = 1/2$, the probability of symbol error after $n = N$ hops conditioned on γ_{S_i} is

$$P_{s|\gamma_{S_i}} = \frac{1}{2} - \frac{1}{2}\prod_{i=1}^{N}\left(1-2p_{i|\gamma_{S_i}}\right). \quad (17)$$

By using (6) and (17), and letting $z = \gamma_{S_i}$, we can obtain the *average* probability of symbol error for the HD relaying case as

$$P_s^{\text{HD}} = \frac{1}{2} - \frac{1}{2}\prod_{i=1}^{N}\left(1-2\mathbb{E}^{\text{HD}}\left[p_{i|\gamma_{S_i}}\right]\right) \quad (18)$$

where $\mathbb{E}^{\text{HD}}[p_{i|\gamma_{S_i}}] = \int_0^\infty p_{i|\gamma_{S_i}} f_{\gamma_{S_i}}^{\text{HD}}(z)\,\text{d}z$. Unfortunately, a closed-form expression for $\mathbb{E}^{\text{HD}}[p_{i|\gamma_{S_i}}]$ cannot be obtained; however, we can use the following lemma to write an approximation for $\mathbb{E}^{\text{HD}}[p_{i|\gamma_{S_i}}]$ when $\alpha = 4$.

Lemma 2: For the high SNR regime, the symbol error probability of ith hop in the HD scenario is, to a good approximation, given by (19), shown at the bottom of the next page.

Proof: See Appendix B. ∎

Similarly by using (7) and (17), the average probability of symbol error for the FD relay is

$$P_s^{\text{FD}} = \frac{1}{2} - \frac{1}{2}\prod_{i=1}^{N}\left(1-2\mathbb{E}^{\text{FD}}\left[p_{i|\gamma_{S_i}}\right]\right). \quad (20)$$

Again, we cannot derive a closed form for (20) due to the difficulty of calculating $\mathbb{E}^{\text{FD}}[p_{i|\gamma_{S_i}}] = \int_0^\infty p_{i|\gamma_{S_i}} f_{\gamma_{S_i}}^{\text{FD}}(z)\,\text{d}z$. However, to obtain a tractable solution and provide insight into the FD scenario, we take an approach that is similar to [11], [25], and [26] and assume that the SI can be reduced to a level R_{SI} that is on the order of thermal noise. Therefore, by using a similar calculation as that in (54), we can recalculate the CDF of γ_{S_i} for the FD case to be

$$F_{\gamma_{S_i}}^{\text{FD}}(z) = 1 - \exp\left(-\frac{z(R_{\text{SI}}+1)d_{i-1,i}^{\alpha}}{P_T}\right)\exp\left(-z^{\frac{2}{\alpha}}\Omega_i\right) \quad (21)$$

and the PDF of γ_{S_i} for the FD case as

$$f_{\gamma_{S_i}}^{\text{FD}}(z) = \left(\frac{2\Omega_i}{\alpha}z^{\frac{2}{\alpha}-1} + \frac{(R_{\text{SI}}+1)d_{i-1,i}^{\alpha}}{P_T}\right) \times \exp\left(-\frac{z(R_{\text{SI}}+1)d_{i-1,i}^{\alpha}}{P_T} - z^{\frac{2}{\alpha}}\Omega_i\right). \quad (22)$$

Then, substituting (22) and (58), the symbol-error probability of the ith hop ($\mathbb{E}^{\text{FD}}[p_{i|\gamma_{S_i}}]$) can be written as (23), shown at the bottom of the next page.

B. Case Study for QPSK

We now focus on QPSK and define that the transition error probability at the receiver in the ith hop is $p_{i,1}$ and $p_{i,2}$ for the nearest-neighbor constellation points and diagonal constellation points, respectively, such that the correct decoding probability is $1 - 2p_{i,1} - p_{i,2}$. From our assumption that the channel gains are exponentially distributed, the symbol-error probability based on the end-to-end SNR at the ith receiver is given by

$$\begin{aligned} p_{i,1|\gamma_{S_i}} &= \frac{1}{2}\,\text{erfc}\left(\sqrt{\gamma_{S_i}}\right) \\ p_{i,2|\gamma_{S_i}} &= \text{erfc}\left(\sqrt{\frac{\gamma_{S_i}}{2}}\right) - \text{erfc}\left(\sqrt{\gamma_{S_i}}\right) - \frac{1}{4}\,\text{erfc}^2\left(\sqrt{\frac{\gamma_{S_i}}{2}}\right) \\ &\overset{\text{(a)}}{\simeq} \left(\frac{e^{-\frac{\gamma_{S_i}}{2}}}{6} + \frac{e^{-\frac{2\gamma_{S_i}}{3}}}{2}\right)\left(1 - \frac{e^{-\frac{\gamma_{S_i}}{2}}}{24} - \frac{e^{-\frac{2\gamma_{S_i}}{3}}}{8}\right) \\ &\quad - \frac{e^{-\gamma_{S_i}}}{6} - \frac{e^{-\frac{4\gamma_{S_i}}{3}}}{2} \end{aligned} \quad (24)$$

where (a) holds by using (57) in Appendix B. Then we can form the following transition matrix for the ith hop:

$$\mathbf{P}_{i|\gamma_{S_i}} = \begin{pmatrix} 1-p_{i,*|\gamma_{S_i}} & p_{i,1|\gamma_{S_i}} & p_{i,1|\gamma_{S_i}} & p_{i,2|\gamma_{S_i}} \\ p_{i,1|\gamma_{S_i}} & 1-p_{i,*|\gamma_{S_i}} & p_{i,2|\gamma_{S_i}} & p_{i,1|\gamma_{S_i}} \\ p_{i,1|\gamma_{S_i}} & p_{i,2|\gamma_{S_i}} & 1-p_{i,*|\gamma_{S_i}} & p_{i,1|\gamma_{S_i}} \\ p_{i,2|\gamma_{S_i}} & p_{i,1|\gamma_{S_i}} & p_{i,1|\gamma_{S_i}} & 1-p_{i,*|\gamma_{S_i}} \end{pmatrix} \quad (25)$$

where $p_{i,*|\gamma_{S_i}} = 2p_{i,1|\gamma_{S_i}} + p_{i,2|\gamma_{S_i}}$. In general, if the prior distribution of the transmitted symbol is given by the vector $\mathbf{p}_0 = (\epsilon_0, \epsilon_1, \epsilon_2, \epsilon_3)^T$, where

$$\begin{aligned} \epsilon_0 &= \mathbb{P}\left(X = \sqrt{P_T/2}(1-j)\right) \\ \epsilon_1 &= \mathbb{P}\left(X = \sqrt{P_T/2}(-1+j)\right) \\ \epsilon_2 &= \mathbb{P}\left(X = \sqrt{P_T/2}(-1-j)\right) \\ \epsilon_3 &= \mathbb{P}\left(X = \sqrt{P_T/2}(1+j)\right) \end{aligned} \quad (26)$$

$$f_{\gamma_{S_i}}^{\text{FD}}(z) = \frac{\left(2P_T\Omega_i\left(d_{i-1,i}^{\alpha}\lambda_{ii}z + P_T\right)z^{\frac{2}{\alpha}} + \left(d_{i-1,i}^{\alpha}\lambda_{ii}z + P_T(\lambda_{ii}+1)\right)\alpha d_{i-1,i}^{\alpha}z\right)e^{-\frac{zd_{i-1,i}^{\alpha}}{P_T} - \Omega_i z^{\frac{2}{\alpha}}}}{\left(d_{i-1,i}^{\alpha}\lambda_{ii}z + P_T\right)^2 \alpha z} \quad (7)$$

and $\sum_{i=0}^{3}\epsilon_i = 1$, then the posterior distribution of decoded symbols at the nth receiver (i.e., after n hops) is

$$\mathbf{p}_n = \mathbf{P}_{n|\gamma_{S_n}} \cdots \mathbf{P}_{1|\gamma_{S_1}} \mathbf{p}_0 = \prod_{i=1}^{n} \mathbf{P}_{i|\gamma_{S_i}} \mathbf{p}_0. \tag{27}$$

The probability that a symbol is decoded erroneously at the nth receiver is

$$\begin{aligned} P_s = {} & \epsilon_0 \mathbb{P}\big(\overline{++}|++\big) + \epsilon_1 \mathbb{P}\big(\overline{+-}|+-\big) \\ & + \epsilon_1 \mathbb{P}\big(\overline{-+}|-+\big) + \epsilon_3 \mathbb{P}\big(\overline{--}|--\big). \end{aligned} \tag{28}$$

The first conditional probability of error after n hops can be written as

$$\mathbb{P}\big(\overline{++}|++\big) = 1 - \mathbf{u}_1^T \mathbf{P}_{n|\gamma_{S_n}} \cdots \mathbf{P}_{1|\gamma_{S_1}} \mathbf{u}_1 \tag{29}$$

where $\mathbf{u}_j$ is the jth column of the 4×4 identity matrix. $\mathbf{P}_{i|\gamma_{S_i}}$ is a symmetric matrix, and can thus be diagonalized. The eigenvalues are $\lambda = 1, 1-4p_{i,1|\gamma_{S_i}}, 1-2p_{i,1|\gamma_{S_i}}-2p_{i,2|\gamma_{S_i}}, 1-2p_{i,1|\gamma_{S_i}}-2p_{i,2|\gamma_{S_i}}$ and the corresponding normalized eigenvectors are

$$\begin{aligned} \mathbf{v}_1 &= (1/2, 1/2, 1/2, 1/2)^T \\ \mathbf{v}_2 &= (1/2, -1/2, -1/2, 1/2)^T \\ \mathbf{v}_3 &= \left(-1/\sqrt{2}, 0, 0, 1/\sqrt{2}\right)^T \\ \mathbf{v}_4 &= \left(0, -1/\sqrt{2}, 1/\sqrt{2}, 0\right)^T. \end{aligned} \tag{30}$$

Hence, we can rewrite the expression given above as

$$\mathbb{P}\big(\overline{++}|++\big) = 1 - \mathbf{u}_1^T \mathbf{V} \mathbf{\Lambda}_n \cdots \mathbf{\Lambda}_1 \mathbf{V}^T \mathbf{u}_1 \tag{31}$$

where $\mathbf{\Lambda}_i = \mathrm{diag}\{1, 1-4p_{i,1|\gamma_{S_i}}, 1-2p_{i,1|\gamma_{S_i}}-2p_{i,2|\gamma_{S_i}}, 1-2p_{i,1|\gamma_{S_i}}-2p_{i,2|\gamma_{S_i}}\}$ and $\mathbf{V} = [\mathbf{v}_1\ \mathbf{v}_2\ \mathbf{v}_3\ \mathbf{v}_4]$. It is thus easy to see that

$$\begin{aligned} \mathbb{P}\big(\overline{++}|++\big) = {} & \frac{3}{4} - \frac{1}{4}\prod_{i=1}^{n}\Big(1-4p_{i,1|\gamma_{S_i}}\Big) \\ & - \frac{1}{2}\prod_{i=1}^{n}\Big(1-2p_{i,1|\gamma_{S_i}}-2p_{i,2|\gamma_{S_i}}\Big). \end{aligned} \tag{32}$$

Similarly, other error probabilities can be written as

$$\begin{aligned} \mathbb{P}\big(\overline{+-}|+-\big) &= \mathbb{P}\big(\overline{-+}|-+\big) = \mathbb{P}\big(\overline{--}|--\big) \\ &= \frac{3}{4} - \frac{1}{4}\prod_{i=1}^{n}\Big(1-4p_{i,1|\gamma_{S_i}}\Big) \\ & \quad - \frac{1}{2}\prod_{i=1}^{n}\Big(1-2p_{i,1|\gamma_{S_i}}-2p_{i,2|\gamma_{S_i}}\Big) \end{aligned} \tag{33}$$

and, for $\epsilon_0 = \epsilon_1 = \epsilon_2 = \epsilon_3 = 1/4$, the probability of symbol error over $n = N$ hops conditioned on γ_{S_i} is

$$\begin{aligned} P_{s|\gamma_{S_i}} = {} & \frac{3}{4} - \frac{1}{4}\prod_{i=1}^{N}\Big(1-4p_{i,1|\gamma_{S_i}}\Big) \\ & - \frac{1}{2}\prod_{i=1}^{N}\Big(1-2p_{i,1|\gamma_{S_i}}-2p_{i,2|\gamma_{S_i}}\Big). \end{aligned} \tag{34}$$

Since, $p_{i|\gamma_{S_i}} = p_{i,1|\gamma_{S_i}}$, by using (6) and (34), and letting $z = \gamma_{S_i}$, we can write the average probability of symbol error

$$\begin{aligned} & \mathbb{E}^{\mathrm{HD}}\Big[p_{i|\gamma_{S_i}}\Big] \\ & \simeq \frac{36}{\sqrt{9\frac{d_{i-1,i}^4}{P_T}+12}\left(\frac{d_{i-1,i}^4}{P_T}+1\right)^{\frac{5}{2}}\left(72\frac{d_{i-1,i}^4}{P_T}+96\right)}\left(\Omega_i\sqrt{\pi}\left(\frac{d_{i-1,i}^4}{P_T}+1\right)^{\frac{5}{2}} e^{\frac{3\Omega_i^2}{12d_{i-1,i}^4/P_T+16}}\mathrm{erfc}\left(\frac{3\Omega_i}{2\sqrt{9\frac{d_{i-1,i}^4}{P_T}+12}}\right)\frac{\sqrt{9\frac{d_{i-1,i}^4}{P_T}+12}}{12}\right. \\ & \left.\times\left(\left(\frac{d_{i-1,i}^4}{P_T}+1\right)\Omega_i\sqrt{\pi}\,\mathrm{erfc}\left(\frac{\Omega_i}{2\sqrt{\frac{d_{i-1,i}^4}{P_T}+1}}\right)\left(\frac{d_{i-1,i}^4}{P_T}+\frac{4}{3}\right)e^{\frac{\Omega_i^2}{4\frac{d_{i-1,i}^4}{P_T}+4}} - 8\left(\frac{d_{i-1,i}^4}{P_T}+1\right)^{\frac{3}{2}}\frac{d_{i-1,i}^4}{P_T}\left(\frac{d_{i-1,i}^4}{P_T}+\frac{13}{12}\right)\right)\right) \end{aligned} \tag{19}$$

$$\begin{aligned} & \mathbb{E}^{\mathrm{FD}}\Big[p_{i|\gamma_{S_i}}\Big] \\ & \simeq \frac{36}{\sqrt{9\frac{(R_{\mathrm{SI}}+1)d_{i-1,i}^4}{P_T}+12}\left(\frac{(R_{\mathrm{SI}}+1)d_{i-1,i}^4}{P_T}+1\right)^{\frac{5}{2}}\left(72\frac{(R_{\mathrm{SI}}+1)d_{i-1,i}^4}{P_T}+96\right)}\left(\Omega_i\sqrt{\pi}\left(\frac{(R_{\mathrm{SI}}+1)d_{i-1,i}^4}{P_T}+1\right)^{\frac{5}{2}} e^{\frac{3\Omega_i^2}{12(R_{\mathrm{SI}}+1)d_{i-1,i}^4/P_T+16}}\right. \\ & \times\mathrm{erfc}\left(\frac{3\Omega_i}{2\sqrt{\frac{9(R_{\mathrm{SI}}+1)d_{i-1,i}^4}{P_T}+12}}\right)\frac{\sqrt{\frac{9(R_{\mathrm{SI}}+1)d_{i-1,i}^4}{P_T}+12}}{12}\left(\left(\frac{(R_{\mathrm{SI}}+1)d_{i-1,i}^4}{P_T}+1\right)\Omega_i\sqrt{\pi}\,\mathrm{erfc}\left(\frac{\Omega_i}{2\sqrt{\frac{(R_{\mathrm{SI}}+1)d_{i-1,i}^4}{P_T}+1}}\right)\right. \\ & \left.\left.\times\left(\frac{(R_{\mathrm{SI}}+1)d_{i-1,i}^4}{P_T}+\frac{4}{3}\right)e^{\frac{\Omega_i^2}{4\frac{(R_{\mathrm{SI}}+1)d_{i-1,i}^4}{P_T}+4}} - 8\left(\frac{(R_{\mathrm{SI}}+1)d_{i-1,i}^4}{P_T}+1\right)^{\frac{3}{2}}\frac{(R_{\mathrm{SI}}+1)d_{i-1,i}^4}{P_T}\left(\frac{(R_{\mathrm{SI}}+1)d_{i-1,i}^4}{P_T}+\frac{13}{12}\right)\right)\right) \end{aligned} \tag{23}$$

for the HD relaying case as

$$P_s^{\mathrm{HD}} = \frac{3}{4} - \frac{1}{4}\prod_{i=1}^{N}\left(1 - 4\mathbb{E}^{\mathrm{HD}}\left[p_{i|\gamma_{S_i}}\right]\right) - \frac{1}{2}\prod_{i=1}^{N}\left(1 - 2\mathbb{E}^{\mathrm{HD}}\left[p_{i|\gamma_{S_i}}\right] - 2\mathbb{E}^{\mathrm{HD}}\left[p_{i,2|\gamma_{S_i}}\right]\right) \quad (35)$$

where

$$\mathbb{E}^{\mathrm{HD}}\left[p_{i,2|\gamma_{S_i}}\right] = \int_0^\infty p_{i,2|\gamma_{S_i}} f_{\gamma_{S_i}}^{\mathrm{HD}}(z)\,\mathrm{d}z. \quad (36)$$

Therefore, when $\alpha = 4$, by substituting (7) and (24) into (36), we can obtain $\mathbb{E}^{\mathrm{HD}}[p_{i,2|\gamma_{S_i}}]$ in (37), shown at the bottom of the next page.

Furthermore, by using (7) and (34), we can obtain the average probability of a symbol error for the FD case as

$$P_s^{\mathrm{FD}} = \frac{3}{4} - \frac{1}{4}\prod_{i=1}^{N}\left(1 - 4\mathbb{E}^{\mathrm{FD}}\left[p_{i|\gamma_{S_i}}\right]\right) - \frac{1}{4}\prod_{i=1}^{N}\left(1 - 2\mathbb{E}^{\mathrm{FD}}\left[p_{i|\gamma_{S_i}}\right] - 2\mathbb{E}^{\mathrm{FD}}\left[p_{i,2|\gamma_{S_i}}\right]\right) \quad (38)$$

where $\mathbb{E}^{\mathrm{FD}}[p_{i,2|\gamma_{S_i}}] = \int_0^\infty p_{i,2|\gamma_{S_i}} f_{\gamma_{S_i}}^{\mathrm{FD}}(z)\,\mathrm{d}z$. By using a similar calculation as before, the $\mathbb{E}[p_{i,2|\gamma_{S_i}}]^{\mathrm{FD}}$ can be obtained in (39), shown at the bottom of the next page.

Remark 2: According to the error probability expressions for the HD and FD modes with BPSK and QPSK, i.e., (18), (20), (35), and (38), respectively, for given $d_{i,i+1}$, the average symbol error probability for the HD relay case depends on the intensity of the third party interferers processes, the path loss exponent α, the transmit power of each node and that of the third part interferers. For the FD case, except for the above parameters, the outage probability is affected by residual SI as well. Further analysis and the effects of these parameters on system performance are presented in Section VI.

V. Asymptotic Analysis

To gain further insight into the performance of multihop systems, we consider two asymptotic regimes: 1) the interference-limited scenario and 2) the noise-limited scenario.

A. Interference-Limited Regime

Consider the case where third-party interference dominates noise and residual SI. The signal-to-interference ratio (SIR) for the HD and FD schemes in this scenario are equivalent

$$\gamma_{S_i}^{\mathrm{HD}} = \gamma_{S_i}^{\mathrm{FD}} = \frac{P_T|h_{i-1,i}|^2/d_{i-1,i}^{\alpha}}{\sum_{m\in\Phi_I} P_I|h_{m,i}|^2/d_{m,i}^{\alpha}}. \quad (40)$$

Note that the equivalence follows from the fact that the level of residual SI is independent of P_I. Letting P_T and P_I grow large with $P_T \gg P_I$, it is easy to see that the corresponding CDFs can be obtained from (4) as

$$F_{\gamma_{S_i}}^{\mathrm{HD}}(z) = F_{\gamma_{S_i}}^{\mathrm{FD}}(z) \sim z^{\frac{2}{\alpha}}\Omega_i \quad (41)$$

and the PDFs become

$$f_{\gamma_{S_i}}^{\mathrm{HD}}(z) = f_{\gamma_{S_i}}^{\mathrm{FD}}(z) \sim \frac{2}{\alpha} z^{\frac{2}{\alpha}-1}\Omega_i \quad (42)$$

where Ω_i was defined in Lemma 1 and the notation $a \sim b$ signifies asymptotic equivalence, i.e., $a/b \to 1$ in the appropriate limit.

1) Outage: Although the PDF and the CDF of the SIR are asymptotically equivalent, the outage probability expressions are not. This discrepancy arises from the fact that FD transmission is much more efficient than HD transmission. Hence, when evaluating the outage probability [see (8)] using the asymptotic CDFs given above, one must set $z = 2^{NR_s} - 1$ for the HD case and $z = 2^{(N+1)R_s/N} - 1$ for the FD case where R_s is the target rate.

2) Error Probability: Let us consider the end-to-end average error probability for BPSK. Referring to (18), we evaluate the expectation[7]

$$\mathbb{E}\left[p_{i|\gamma_{S_i}}\right] = \frac{1}{2}\int_0^\infty \mathrm{erfc}\left(\sqrt{\gamma_{S_i}}\right) f_{\gamma_{S_i}}(\gamma_{S_i})\,\mathrm{d}\gamma_{S_i} \sim \frac{\Omega_i \Gamma\left(\frac{1}{2}+\frac{2}{\alpha}\right)}{2\sqrt{\pi}}. \quad (43)$$

It follows that for large P_T/P_I, the average end-to-end error probability for BPSK is asymptotically

$$P_s \sim \frac{1}{2} - \frac{1}{2}\prod_{i=1}^{N}\left(1 - \frac{\Omega_i \Gamma\left(\frac{1}{2}+\frac{2}{\alpha}\right)}{\sqrt{\pi}}\right) \sim \frac{\sqrt{\pi}\rho_M \Gamma\left(\frac{1}{2}+\frac{2}{\alpha}\right)}{2\,\mathrm{sinc}\left(\frac{2}{\alpha}\right)}\left(\frac{P_I}{P_T}\right)^{\frac{2}{\alpha}}\sum_{i=1}^{N} d_{i-1,i}^2. \quad (44)$$

From this expression, we can easily observe a quadratic dependence on distance and a linear dependence on interference density, as well as a $2/\alpha$ power-law decay in the error probability with increasing P_T/P_I.

A similar approach is taken to analyze the symbol error probability for QPSK. Referring to (35), we require an expression for $\mathbb{E}[p_{i,1|\gamma_{S_i}}]$, which is given by (43). Furthermore, we require the slightly more complicated result

$$\mathbb{E}\left[p_{i,2|\gamma_{S_i}}\right] \sim \frac{\Omega_i}{\pi}\left(\sqrt{\pi}\left(4^{1/\alpha}-1\right)\Gamma\left(\frac{1}{2}+\frac{2}{\alpha}\right) - \frac{\Gamma\left(\frac{2}{\alpha}\right)}{\alpha+4}\,{}_2F_1\left(1, \frac{\alpha+2}{\alpha}; \frac{3}{2}+\frac{2}{\alpha}; \frac{1}{2}\right)\right) \quad (45)$$

where ${}_2F_1(a,b;c;z) = [\Gamma(c)/(\Gamma(c)\Gamma(c-b))]\int_0^1 [(t^{b-1}(1-t)^{c-b-1})/((1-tz)^a)]\mathrm{d}t$ is the hypergeometric function. This expression follows from direct integration, where the $\mathrm{erfc}(\cdot)^2$ integral is evaluated by using integration by parts, a change of variables, and using [27, eq. (6.455 2)] along with a few algebraic manipulations. Substituting these expectations into (35)

[7]We omit the superscripts HD and FD in this analysis since there is no distinction between the SIR distribution in this asymptotic analysis.

and letting P_T/P_I grow large, we have the asymptotic relation

$$P_s \sim \left(\frac{4^{1/\alpha}\Gamma\left(\frac{1}{2}+\frac{2}{\alpha}\right)}{\sqrt{\pi}} - \frac{\Gamma\left(\frac{2}{\alpha}\right) {}_2F_1\left(1,\, \frac{\alpha+2}{\alpha};\, \frac{3}{2}+\frac{2}{\alpha};\, \frac{1}{2}\right)}{\pi(\alpha+4)} \right) \times \frac{\pi\rho_M}{\operatorname{sinc}\left(\frac{2}{\alpha}\right)} \left(\frac{P_I}{P_T}\right)^{\frac{2}{\alpha}} \sum_{i=1}^{N} d_{i-1,i}^2 \tag{46}$$

for QPSK. The only major difference between the QPSK symbol error probability expression and the corresponding result

$$\begin{aligned}
\mathbb{E}^{\mathrm{HD}}\left[p_{i,2|\gamma_{S_i}}\right] \simeq{}& \frac{\sqrt{\pi}\Omega_i e^{\frac{3\Omega_i^2}{12\frac{d_{i-1,i}^4}{P_T}+8}} \operatorname{erfc}\left(\frac{3\Omega_i}{2\sqrt{9\frac{d_{i-1,i}^4}{P_T}+6}}\right)}{6\left(\frac{d_{i-1,i}^4}{P_T}+\frac{2}{3}\right)^{\frac{3}{2}}} + \frac{\sqrt{\pi}\Omega_i e^{\frac{\Omega_i^2}{4\frac{d_{i-1,i}^4}{P_T}+2}} \operatorname{erfc}\left(\frac{\Omega_i}{2\sqrt{4\frac{d_{i-1,i}^4}{P_T}+2}}\right)}{6\sqrt{2}\left(\frac{2d_{i-1,i}^4}{P_T}+1\right)^{\frac{3}{2}}} + \frac{4\frac{d_{i-1,i}^4}{P_T}\left(\frac{d_{i-1,i}^4}{P_T}+\frac{13}{24}\right)}{\left(\frac{2d_{i-1,i}^4}{P_T}+1\right)\left(\frac{3d_{i-1,i}^4}{P_T}+2\right)} \\
&- 2p_i^{\mathrm{HD}} - \frac{7\sqrt{\pi}\Omega_i\left(\frac{d_{i-1,i}^4}{P_T}+\frac{4}{3}\right)e^{\frac{3\Omega_i^2}{12\frac{d_{i-1,i}^4}{P_T}+14}} \operatorname{erfc}\left(\frac{3\Omega_i}{2\sqrt{36\frac{d_{i-1,i}^4}{P_T}+42}}\right)}{16\sqrt{\frac{d_{i-1,i}^4}{P_T}+\frac{7}{6}}\left(\frac{18d_{i-1,i}^8}{P_T^2}+\frac{45d_{i-1,i}^4}{P_T}+28\right)} - \frac{\frac{288d_{i-1,i}^{12}}{P_T^3}+\frac{648d_{i-1,i}^8}{P_T^2}+\frac{361d_{i-1,i}^4}{P_T}}{\frac{2592d_{i-1,i}^{12}}{P_T^3}+\frac{9072d_{i-1,i}^8}{P_T^2}+10512\frac{d_{i-1,i}^4}{P_T}+4032} \\
&- \frac{\sqrt{\pi}\Omega_i\left(\frac{d_{i-1,i}^4}{P_T}+\frac{4}{3}\right)\left(\frac{d_{i-1,i}^4}{P_T}+\frac{7}{6}\right)e^{\frac{\Omega_i^2}{4\frac{d_{i-1,i}^4}{P_T}+4}} \operatorname{erfc}\left(\frac{\Omega_i}{2\sqrt{\frac{d_{i-1,i}^4}{P_T}+1}}\right)}{16\left(\frac{d_{i-1,i}^4}{P_T}+1\right)^{\frac{3}{2}}\left(\frac{18d_{i-1,i}^8}{P_T^2}+\frac{45d_{i-1,i}^4}{P_T}+28\right)} - \frac{3\sqrt{\pi}\Omega_i\left(\frac{d_{i-1,i}^4}{P_T}+\frac{7}{6}\right)e^{\frac{3\Omega_i^2}{12\frac{d_{i-1,i}^4}{P_T}+16}} \operatorname{erfc}\left(\frac{3\Omega_i}{2\sqrt{9\frac{d_{i-1,i}^4}{P_T}+12}}\right)}{4\sqrt{\frac{d_{i-1,i}^4}{P_T}+\frac{4}{3}}\left(\frac{18d_{i-1,i}^8}{P_T^2}+\frac{45d_{i-1,i}^4}{P_T}+28\right)}
\end{aligned} \tag{37}$$

$$\begin{aligned}
\mathbb{E}\left[p_{i,2|\gamma_{S_i}}\right]^{\mathrm{FD}} \simeq{}& \frac{\sqrt{\pi}\Omega_i e^{\frac{3\Omega_i^2}{12\frac{(R_{\mathrm{SI}}+1)d_{i-1,i}^4}{P_T}+8}} \operatorname{erfc}\left(\frac{3\Omega_i}{2\sqrt{9\frac{(R_{\mathrm{SI}}+1)d_{i-1,i}^4}{P_T}+6}}\right)}{6\left(\frac{(R_{\mathrm{SI}}+1)d_{i-1,i}^4}{P_T}+\frac{2}{3}\right)^{\frac{3}{2}}} + \frac{\sqrt{\pi}\Omega_i e^{\frac{\Omega_i^2}{4\frac{(R_{\mathrm{SI}}+1)d_{i-1,i}^4}{P_T}+2}} \operatorname{erfc}\left(\frac{\Omega_i}{2\sqrt{4\frac{(R_{\mathrm{SI}}+1)d_{i-1,i}^4}{P_T}+2}}\right)}{6\sqrt{2}\left(\frac{2(R_{\mathrm{SI}}+1)d_{i-1,i}^4}{P_T}+1\right)^{\frac{3}{2}}} - 2p_i^{\mathrm{HD}} \\
&+ \frac{4\frac{(R_{\mathrm{SI}}+1)d_{i-1,i}^4}{P_T}\left(\frac{(R_{\mathrm{SI}}+1)d_{i-1,i}^4}{P_T}+\frac{13}{24}\right)}{\left(\frac{2(R_{\mathrm{SI}}+1)d_{i-1,i}^4}{P_T}+1\right)\left(\frac{3(R_{\mathrm{SI}}+1)d_{i-1,i}^4}{P_T}+2\right)} - \frac{7\sqrt{\pi}\Omega_i\left(\frac{(R_{\mathrm{SI}}+1)d_{i-1,i}^4}{P_T}+\frac{4}{3}\right)e^{\frac{3\Omega_i^2}{12\frac{(R_{\mathrm{SI}}+1)d_{i-1,i}^4}{P_T}+14}} \operatorname{erfc}\left(\frac{3\Omega_i}{2\sqrt{36\frac{(R_{\mathrm{SI}}+1)d_{i-1,i}^4}{P_T}+42}}\right)}{16\sqrt{\frac{(R_{\mathrm{SI}}+1)d_{i-1,i}^4}{P_T}+\frac{7}{6}}\left(\frac{18(R_{\mathrm{SI}}+1)^2d_{i-1,i}^8}{P_T^2}+\frac{45(R_{\mathrm{SI}}+1)d_{i-1,i}^4}{P_T}+28\right)} \\
&- \frac{\frac{288(R_{\mathrm{SI}}+1)^3d_{i-1,i}^{12}}{P_T^3}+\frac{648(R_{\mathrm{SI}}+1)^2d_{i-1,i}^8}{P_T^2}+\frac{361(R_{\mathrm{SI}}+1)d_{i-1,i}^4}{P_T}}{\frac{2592(R_{\mathrm{SI}}+1)^3d_{i-1,i}^{12}}{P_T^3}+\frac{9072(R_{\mathrm{SI}}+1)^2d_{i-1,i}^8}{P_T^2}+10512\frac{(R_{\mathrm{SI}}+1)d_{i-1,i}^4}{P_T}+4032} \\
&- \frac{\sqrt{\pi}\Omega_i\left(\frac{(R_{\mathrm{SI}}+1)d_{i-1,i}^4}{P_T}+\frac{4}{3}\right)\left(\frac{(R_{\mathrm{SI}}+1)d_{i-1,i}^4}{P_T}+\frac{7}{6}\right)e^{\frac{\Omega_i^2}{4\frac{(R_{\mathrm{SI}}+1)d_{i-1,i}^4}{P_T}+4}} \operatorname{erfc}\left(\frac{\Omega_i}{2\sqrt{\frac{(R_{\mathrm{SI}}+1)d_{i-1,i}^4}{P_T}+1}}\right)}{16\left(\frac{(R_{\mathrm{SI}}+1)d_{i-1,i}^4}{P_T}+1\right)^{\frac{3}{2}}\left(\frac{18(R_{\mathrm{SI}}+1)^2d_{i-1,i}^8}{P_T^2}+\frac{45(R_{\mathrm{SI}}+1)d_{i-1,i}^4}{P_T}+28\right)} \\
&- \frac{3\sqrt{\pi}\Omega_i\left(\frac{(R_{\mathrm{SI}}+1)d_{i-1,i}^4}{P_T}+\frac{7}{6}\right)e^{\frac{3\Omega_i^2}{12\frac{(R_{\mathrm{SI}}+1)d_{i-1,i}^4}{P_T}+16}} \operatorname{erfc}\left(\frac{3\Omega_i}{2\sqrt{9\frac{(R_{\mathrm{SI}}+1)d_{i-1,i}^4}{P_T}+12}}\right)}{4\sqrt{\frac{(R_{\mathrm{SI}}+1)d_{i-1,i}^4}{P_T}+\frac{4}{3}}\left(\frac{18(R_{\mathrm{SI}}+1)^2d_{i-1,i}^8}{P_T^2}+\frac{45(R_{\mathrm{SI}}+1)d_{i-1,i}^4}{P_T}+28\right)}
\end{aligned} \tag{39}$$

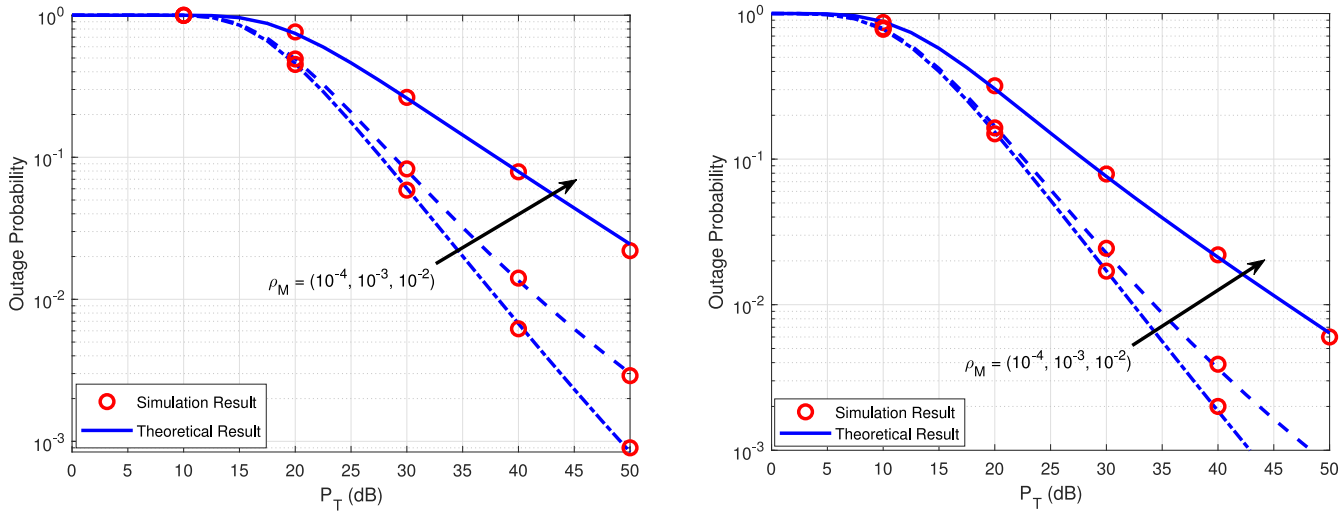

Fig. 2. Theoretical versus numerical outage probabilities for different density of interferers, where $N = 5$, $P_I = 20$ dB, $\lambda_{ii} = 5$ dB, and $\alpha = 4$. (a) HD case. (b) FD case.

for BPSK is the factor in the parentheses in the first line of the asymptotic equivalence given above. However, this factor only depends upon the path loss exponent; hence, we observe the same linear dependence on the interference density and power-law decay with increasing SIR as we did for BPSK, as one would expect.

B. Noise-Limited Regime

Let us turn our attention to the noise-limited regime. This case is akin to setting P_I and $\gamma_{i,i}$ to zero in (2) and (3).[8] It follows that the SNR for the HD and FD systems can be written as:

$$\gamma_{S_i}^{\mathrm{HD}} = \gamma_{S_i}^{\mathrm{FD}} = \frac{P_T |h_{i-1,i}|^2}{d_{i-1,i}^{\alpha}}. \tag{47}$$

Furthermore, by letting the SNR grow large (i.e., $P_T \to \infty$), we can deduce that the PDFs and CDFs of the SNR obey the following asymptotic equivalences:

$$\begin{aligned} F_{\gamma_{S_i}}^{\mathrm{HD}}(z) &= F_{\gamma_{S_i}}^{\mathrm{FD}}(z) \sim \frac{z d_{i-1,i}^{\alpha}}{P_T} \\ f_{\gamma_{S_i}}^{\mathrm{HD}}(z) &= f_{\gamma_{S_i}}^{\mathrm{FD}}(z) \sim \frac{d_{i-1,i}^{\alpha}}{P_T}. \end{aligned} \tag{48}$$

1) Outage: As noted in the discussion of the interference-limited regime, the outage probability expressions for HD and FD systems are identical, despite the fact that the SNR distributions are asymptotically equivalent. By substituting the CDF into (8), one observes that the outage probability is

$$P_o \sim \frac{z}{P_T} \sum_{i=1}^{N} d_{i-1,i}^{\alpha}, \ \ P_T \to \infty \tag{49}$$

for the noise-limited regime.

2) Error Probability: For the error probability analysis, we again begin with a study of BPSK. We evaluate the required expectation to give

$$\mathbb{E}\Big[p_{i|\gamma_{S_i}}\Big] \sim \frac{d_{i-1,i}^{\alpha}}{4P_T}. \tag{50}$$

The resulting high-SNR expression for the end-to-end average error probability is

$$P_s \sim \frac{1}{4P_T} \sum_{i=1}^{N} d_{i-1,i}^{\alpha}. \tag{51}$$

This analysis confirms that, as one would expect, the diversity order of the system is one. Moreover, it demonstrates the dependence on the α-powers of distances between nodes.

Turning our attention to QPSK, we require $\mathbb{E}[p_{i,1|\gamma_{S_i}}]$, which is given by (50). We also need the asymptotic relation

$$\mathbb{E}\Big[p_{i,2|\gamma_{S_i}}\Big] \sim \frac{2+\pi}{4\pi} \frac{d_{i-1,i}^{\alpha}}{P_T} \tag{52}$$

which can be computed in a similar manner to (45), using [28, eq. (15.4.29)] to simplify the expression of the hypergeometric function. Substituting into (35) and letting P_T/P_I grow large, we have

$$P_s \sim \frac{2+3\pi}{4\pi P_T} \sum_{i=1}^{N} d_{i-1,i}^{\alpha} \tag{53}$$

from which the same scaling in SNR and α noted for BPSK can be observed. Furthermore, note that the asymptotic error probability expressions for BPSK and QPSK differ by the factors $1/4$ and $(2+3\pi)/(4\pi) \simeq 0.91$, i.e., the high-SNR coding gain for BPSK is roughly 3.6 times better than that of QPSK.

VI. Simulations Results

This section provides Monte Carlo simulation results to verify the proposed theoretical analysis for the outage and error probability, respectively. In the simulations, without loss of generality, we assume the noise variance $\sigma_n^2 = 1$, the target rate $R_s = 1$ bits/s/Hz, and the locations of the transmitter and

[8] We let $\gamma_{i,i} = 0$ here, since, as noted before, state-of-the-art SI cancellation methods can reduce interference to the noise floor. Thus, omitting $\gamma_{i,i}$ from the expression does not affect the ensuing analysis.

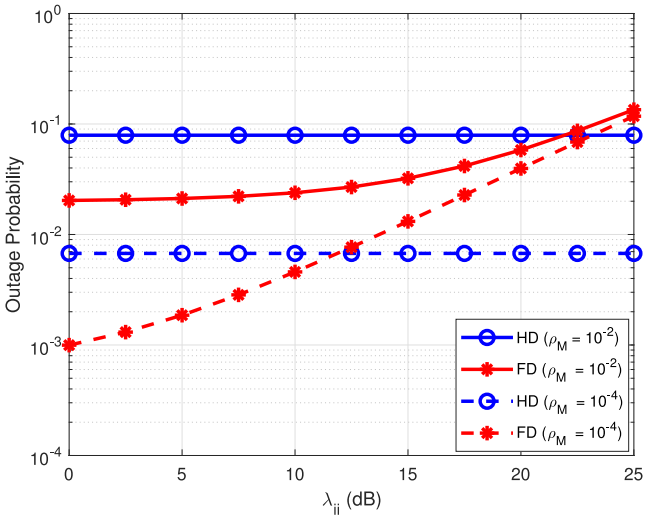

Fig. 3. Comparison of outage probabilities for FD and HD relaying with different residual SI channel gains, where $N = 5$, $P_T = 40$ dB, $P_I = 20$ dB, and $\alpha = 4$.

receiver are fixed at $(-2, 0)$ and $(2, 0)$, respectively. The simulation results are obtained by averaging over 10^5 independent trials. For the case of randomly located interferers, we model the interferers as a homogeneous PPP Φ_I with density ρ_I. The comparison of outage and error probability between the HD and FD cases will be investigated.

A. Outage Probability

Fig. 2 verifies the outage probability expressions for HD and FD relaying versus different density of interferers, where $N = 5$, $P_I = 20$ dB, $\lambda_{ii} = 5$ dB, and $\alpha = 4$. Both the simulation and the theoretical results are presented, which are shown to match perfectly. Furthermore, for both the HD and FD cases, it is clear that the outage probability decreases as the transmit power to noise ratio of internode increases; and the outage probability increases when the density of interferers increases.

According to [24], radio transmissions always encounter a bandwidth constraint so that SI cannot always be cancelled completely. Therefore, it is fairly important to show how residual SI affects the outage performance of the FD scheme. Fig. 3 compares the outage probabilities for the HD and FD modes with respect to different λ_{ii}, where $N = 5$, $P_T = 40$ dB, $P_I = 20$ dB, and $\alpha = 4$. It is clearly shown that as the residual SI increases, the outage probability of the FD case is adversely affected. There is no SI for the HD scheme; hence, the performance is constant for all λ_{ii} in this figure. This information can be employed in practice to switch between HD and FD modes given the bandwidth constraints of the system. Since the available system bandwidth of modern communication links can change based on channel quality and the prescribed quality of service, this observation could be of great importance in multihop IoT.

B. Error Probability

Fig. 4 provides the comparison of error probability of BPSK and QPSK for HD relaying with a different number of hops and density of the interferers, where $P_I = 30$ dB and $\alpha = 4$.

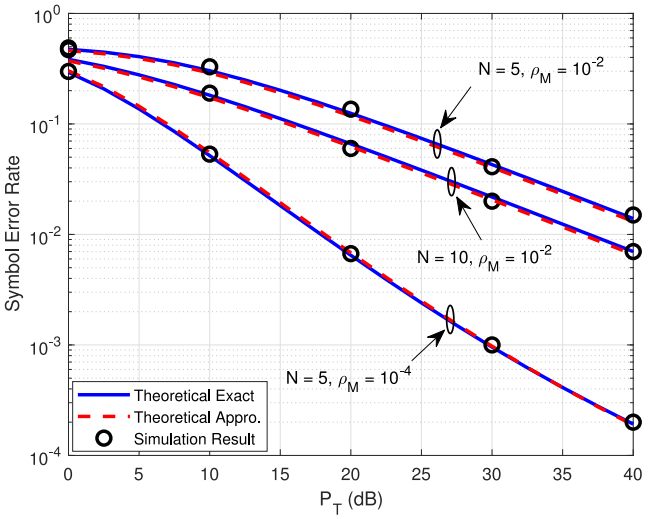

(a)

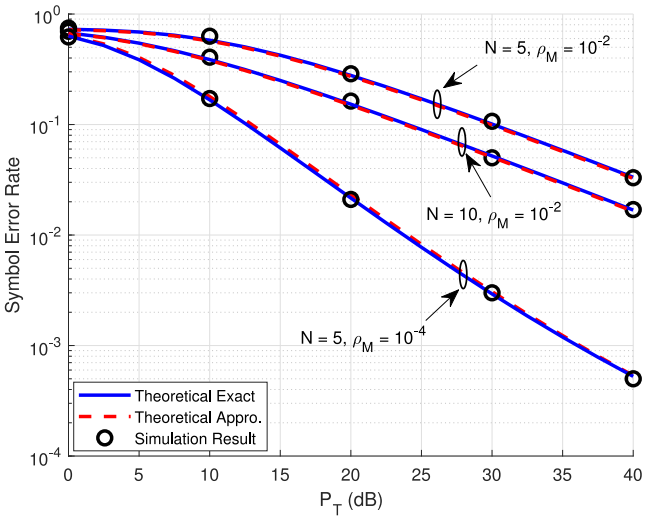

(b)

Fig. 4. Theoretical versus numerical results for HD relaying with different number of hops and density of interferers, where $P_I = 30$ dB and $\alpha = 4$. (a) BPSK. (b) QPSK.

The simulation, exact theoretical and approximation results are provided. It is clear to see that the approximation results match well with the simulation results, which verifies the proposed Markov Chain model can be used to accurately analyze the end-to-end error probability. Moreover, the error probability decreases as the transmit power to noise ratio of internodes increases for both BPSK and QPSK. With increase in the density of the interferers, the error probability for both cases increases. For example, when $P_T = 30$ dB and $N = 5$, the BER for BPSK are almost 0.04 and 0.001 for the density of interferers $\rho_M = 10^{-2}$ m^{-2} and $\rho_M = 10^{-2}$ m^{-2}, respectively. Furthermore, with the increasing number of hops, the error probability decreases. In other words, we can use more relays to help the source forward the signal to the destination so that the distance between two neighbor nodes is reduced, and the error probability of each transmission hop is decreased. For example, when $P_T = 30$ dB and $\rho_M = 10^{-2}$ m^{-2}, the SER will decrease from 0.1 to 0.04 for $N = 5$ to $N = 10$.

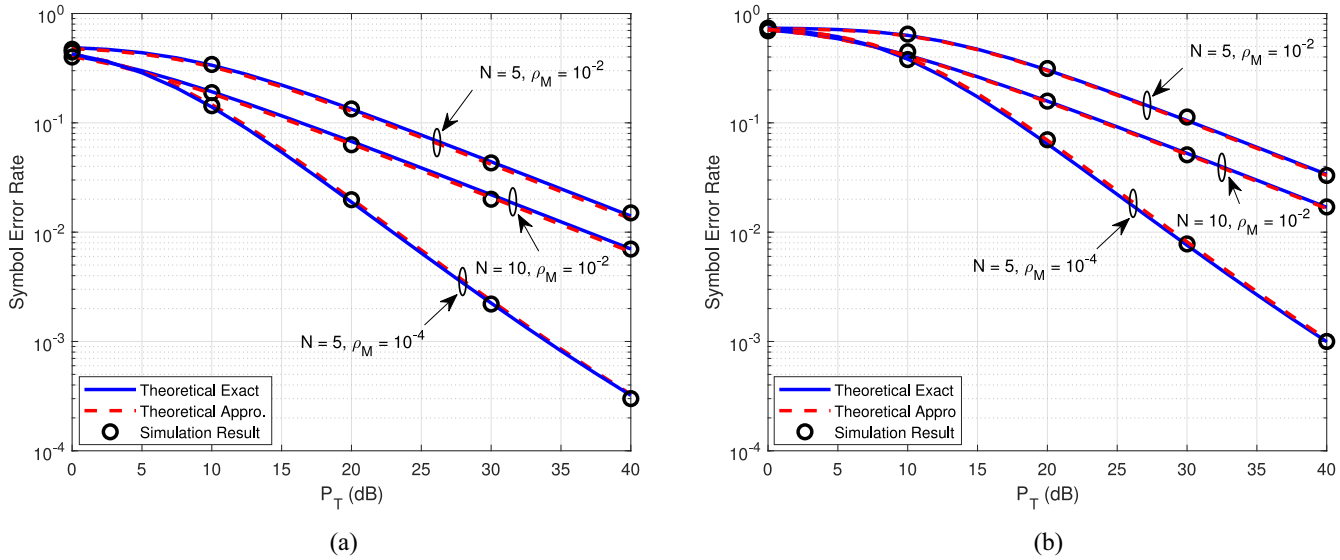

Fig. 5. Theoretical versus numerical results for FD relaying with different number of hops and density of interferers, where $P_I = 30$ dB, $\lambda_{ii} = 5$ dB, and $\alpha = 4$. (a) BPSK. (b) QPSK.

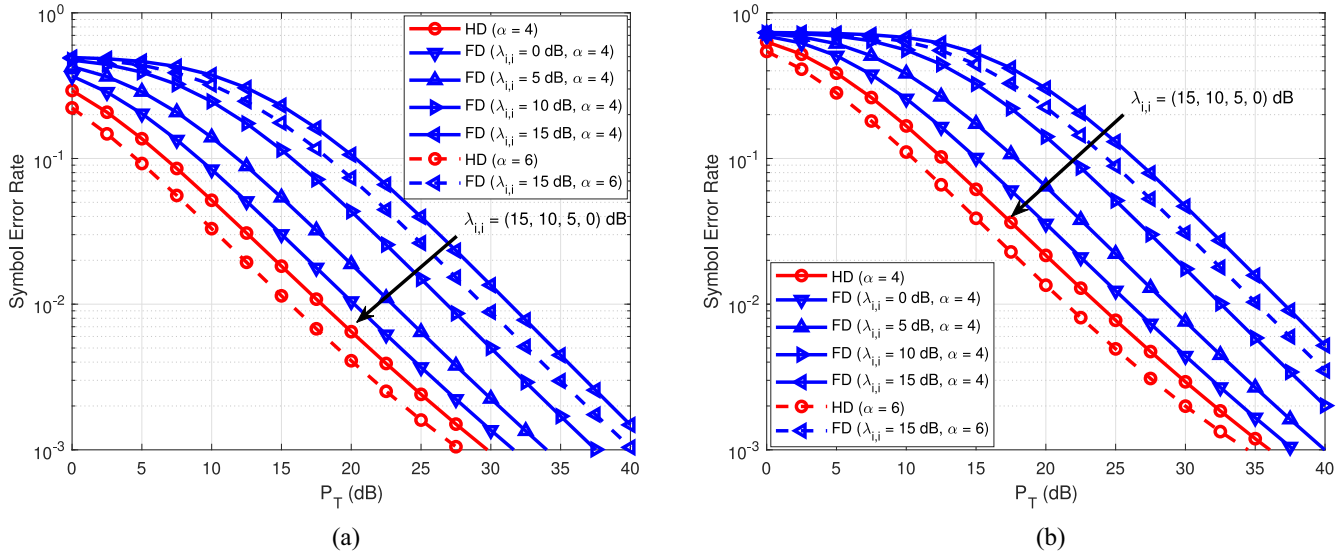

Fig. 6. Comparison of error rate between FD and HD relaying with different residual SI channel gains, where $N = 5$, $P_I = 30$ dB, and $\rho_M = 10^{-4}$ m^{-2}. (a) BPSK. (b) QPSK.

The comparison between theoretical and simulation results corresponding to FD relaying for BPSK and QPSK are illustrated in Fig. 5. Here, we let $P_I = 30$ dB, $\lambda_{ii} = 5$ dB, and $\alpha = 4$. Again, the theoretical approximation results are well matched to the simulation and exact theoretical results. The expected trends are observed that the error probability increases with the intensity of interferers and decreases with increasing numbers of hops.

Fig. 6 shows the comparison of the error probability between HD and FD relaying versus different residual SI and path loss exponents, where $\rho_M = 10^{-4}$ m^{-2}, $P_I = 30$ dB, and $N = 5$. It is clear to see that the SER of both the HD and FD cases decreases when the path loss exponent increases. Physically, this result implies that cluttered environments exhibiting high propagation losses are more beneficial for the multihop transmission with a short distance. Furthermore, we can see that by increasing the residual SI, the error probability of the FD case increases. According to [11], the SI can be reduced to the noise floor. Therefore, the error probability of HD is the lower bound for that of FD. For the multihop IoT, a natural question is how to achieve the optimal outage and error probability by using the HD and FD scenario according to the residual SI? The answer to this question can be shown in Figs. 3 and 6. For example, when the error probability is considered high priority in the multihop system, the HD mode should be utilized to obtain the optimal system performance. In contrast, for the FD mode, a low level of residual SI is required to achieve better outage performance.

C. Asymptotic Results

Fig. 7 shows the comparison of error rate between the exact and asymptotic results for the interference-limited case, where $N = 5$, $P_I = 20$ dB, $\rho_M = 10^{-4}$ m^{-2}, $\lambda_{ii} = 0$ dB, and $\alpha = 4$.

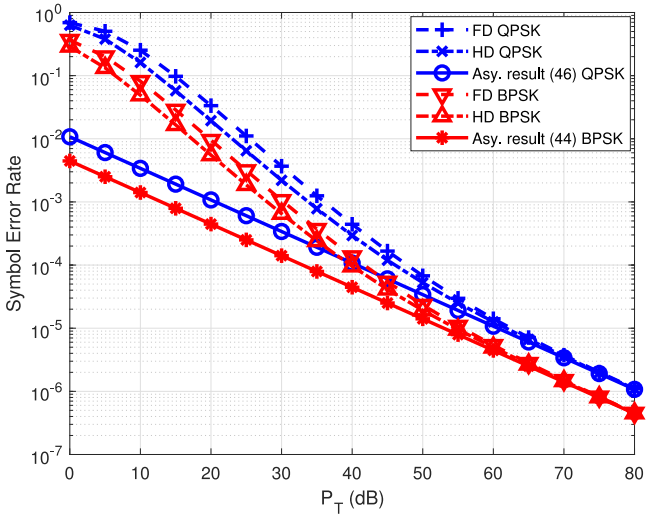

Fig. 7. Comparison of error rate between the exact and asymptotic results for the interference-limited case, where $N = 5$, $P_I = 20$ dB, $\rho_M = 10^{-4}$ m^{-2}, $\lambda_{ii} = 0$ dB, and $\alpha = 4$.

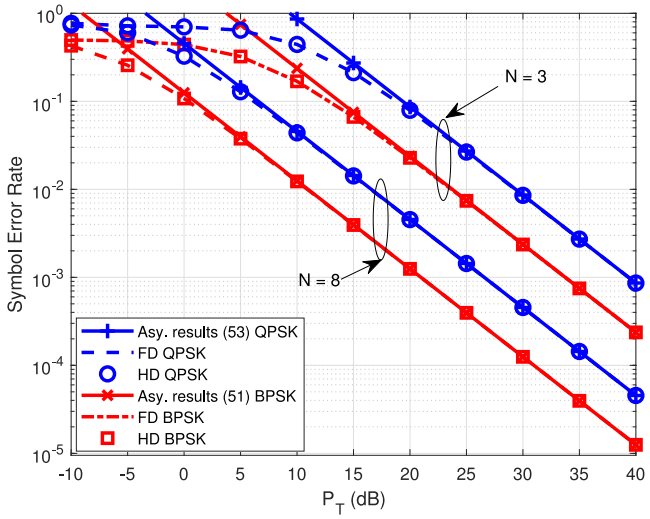

Fig. 8. Comparison of error rate between the exact and asymptotic results for the noise-limited case, where $P_I = 0$, $\rho_M = 10^{-4}$ m^{-2}, $\lambda_{ii} = 0$, and $\alpha = 4$.

We can see that with increasing the transmit power to noise ratio P_T, the error probability of the exact results for both FD and HD cases achieve to the asymptotic results for both BPSK and QPSK. Furthermore, as mentioned before, for BPSK and QPSK, the same linear dependence on the interference density and power-law decay with increasing SIR. Fig. 8 shows the comparison of error rate between the exact and asymptotic results for the noise-limited case, where $P_I = 0$, $\rho_M = 10^{-4}$ m^{-2}, $\lambda_{ii} = 0$, and $\alpha = 4$. Again with increasing the transmit power to noise ratio P_T, the error probability of the exact results for both FD and HD cases achieve to the asymptotic results for both BPSK and QPSK. Furthermore, there are the diversity orders of BPSK and QPSK are one and the coding gain can be achieved by considering BPSK as we expect.

VII. Conclusion

In this paper, HD and FD DF relaying schemes were considered in multihop IoT networks in the presence of randomly located interferers, where the locations of the interferers are modeled by a PPP. We derived closed-form expressions for the outage probability and approximations of the SER for the HD and FD transmission by using a Markov Chain Model for different modulations. The derived analytical results were verified by using Monte Carlo simulations and it was shown that HD and FD transmission can be used to obtain the optimal performance in terms of the outage and error probability, according to different levels of residual SI and the density of the interferers. In the future, it would be interesting to consider a power allocation method to obtain the transmit power of the node to obtain the optimal system performance.

Appendix A

First, the CDF of (2) can be obtained as

$$\begin{aligned}
F^{\mathrm{HD}}_{\gamma_{S_i}}(z) &= \mathbb{P}\left(\frac{\frac{P_T|h_{i-1,i}|^2}{d^{\alpha}_{i-1,i}}}{\sum\limits_{m\in\Phi_I}\frac{P_I|h_{m,i}|^2}{d^{\alpha}_{m,i}}+1} < z\right)\\
&= \mathbb{P}\left(\frac{P_T|h_{i-1,i}|^2}{d^{\alpha}_{i-1,i}} - z < z\sum_{m\in\Phi_I}\frac{P_I|h_{m,i}|^2}{d^{\alpha}_{m,i}}\right)\\
&= 1-\exp\left(-\frac{zd^{\alpha}_{i-1,i}}{P_T}\right)\mathbb{E}\left[\prod_{m\in\Phi_I} e^{-z\frac{P_I}{P_T}|h_{m,i}|^2 d^{\alpha}_{i-1,i}d^{-\alpha}_{m,i}}\right]\\
&\overset{(a)}{=} 1-\exp\left(-\frac{zd^{\alpha}_{i-1,i}}{P_T}\right)\mathbb{E}_{\Phi_I}\\
&\quad\times\left[\prod_{m\in\Phi_I}\int_0^{\infty} e^{-zd^{\alpha}_{i-1,i}\frac{P_I}{P_T}sd^{-\alpha}_{m,i}}e^{-s}\,\mathrm{d}s\right]\\
&= 1-\exp\left(-\frac{zd^{\alpha}_{i-1,i}}{P_T}\right)\mathbb{E}_{\Phi_I}\left[\prod_{m\in\Phi_I}\frac{1}{1+\frac{P_I}{P_T}z\left(d_{i-1,i}/d_{m,i}\right)^{\alpha}}\right]\\
&\overset{(b)}{=} 1-\exp\left(-\frac{zd^{\alpha}_{i-1,i}}{P_T}\right)\\
&\quad\times\exp\left(\rho_M\int_0^{2\pi}\int_0^{\infty}\left(\frac{-\frac{P_I}{P_T}z\left(d_{i-1,i}/r\right)^{\alpha}}{1+\frac{P_I}{P_T}z\left(d_{i-1,i}/r\right)^{\alpha}}\right)r\,\mathrm{d}r\,\mathrm{d}\theta\right)\\
&= 1-\exp\left(-\frac{zd^{\alpha}_{i-1,i}}{P_T}\right)\exp\left(-z^{\frac{2}{\alpha}}\Omega_i\right) \qquad (54)
\end{aligned}$$

where for (a), we let $s = |h_{i-1,i}|^2$ and the PDF of s be $f_s(s) = e^{-s}$, and (b) holds for the probability generating functional.

Then the CDF of (3) for the FD relaying case can be obtained as (55), shown at the top of the next page, where $\Psi = [(P_T e^{-([d^{\alpha}_{i-1,i}z]/P_T)})/(d^{\alpha}_{i-1,i}\lambda_{ii}z + P_T)]$. For (a), let $X = [(P_T|h_{i-1,i}|^2)/(d^{\alpha}_{i-1,i})]$ and $Y = z\gamma_{i,i}$, therefore the CDF of $T = X - Y - z$ is

$$\begin{aligned}
F_T(t) &= \int_0^{\infty}\int_0^{t+y+z}\frac{d^{\alpha}_{i-1,i}}{P_T}e^{-\frac{xd^{\alpha}_{i-1,i}}{P_T}}\frac{1}{\lambda_{ii}z}e^{-\frac{y}{\lambda_{ii}z}}\,\mathrm{d}x\,\mathrm{d}y\\
&= 1-\Psi e^{-t\frac{d^{\alpha}_{i-1,i}}{P_T}} \qquad (56)
\end{aligned}$$

in (b), we let $s = |h_{i-1,i}|^2$ and the PDF of s is $f_s(s) = e^{-s}$, and (c) holds for the probability generating functional.

$$
\begin{aligned}
F_{\gamma_{S_i}}^{\mathrm{FD}}(z) &= \mathbb{P}\left(\frac{\frac{P_T|h_{i-1,i}|^2}{d_{i-1,i}^{\alpha}}}{\sum_{m\in\Phi_I}\frac{P_I|h_{m,i}|^2}{d_{m,i}^{\alpha}}+\gamma_{i,i}+1}<z\right)=\mathbb{P}\left(\frac{P_T|h_{i-1,i}|^2}{d_{i-1,i}^{\alpha}}-z\gamma_{i,i}-z<z\sum_{m\in\Phi_I}\frac{P_I|h_{m,i}|^2}{d_{m,i}^{\alpha}}\right)\\
&\overset{(a)}{=} 1-\Psi\mathbb{E}\left[\prod_{m\in\Phi_I}e^{-z\frac{P_I}{P_T}|h_{m,i}|^2 d_{i-1,i}^{\alpha}d_{m,i}^{-\alpha}}\right]\\
&\overset{(b)}{=} 1-\Psi\mathbb{E}_{\Phi_I}\left[\prod_{m\in\Phi_I}\int_0^{\infty}e^{-zd_{i-1,i}^{\alpha}\frac{P_I}{P_T}sd_{m,i}^{-\alpha}}e^{-s}\,\mathrm{d}s\right]\\
&= 1-\Psi\mathbb{E}_{\Phi_I}\left[\prod_{m\in\Phi_I}\frac{1}{1+\frac{P_I}{P_T}z\left(d_{i-1,i}/d_{m,i}\right)^{\alpha}}\right]\\
&\overset{(c)}{=} 1-\Psi\exp\left(\rho_M\int_0^{2\pi}\int_0^{\infty}\left(\frac{-\frac{P_I}{P_T}z\left(d_{i-1,i}/r\right)^{\alpha}}{1+\frac{P_I}{P_T}z\left(d_{i-1,i}/r\right)^{\alpha}}\right)r\,\mathrm{d}r\,\mathrm{d}\theta\right)=1-\Psi\exp\left(-z^{\frac{2}{\alpha}}\Omega_i\right)
\end{aligned}
\tag{55}
$$

APPENDIX B

According to [29], when $x>0$ we have

$$
Q(x)=\frac{1}{2}\operatorname{erfc}\left(\frac{x}{\sqrt{2}}\right)\simeq\frac{1}{12}e^{-\frac{x^2}{2}}+\frac{1}{4}e^{-\frac{2x^2}{3}} \tag{57}
$$

where $Q(x)=(1/\sqrt{2\pi})\int_x^{\infty}e^{-(u^2/2)}\,\mathrm{d}u$ denotes the Q-function. Therefore, we can get

$$
p_{i|\gamma_{S_i}}=\frac{1}{2}\operatorname{erfc}\left(\sqrt{x}\right)=Q\left(\sqrt{2x}\right)\simeq\frac{1}{12}e^{-x}+\frac{1}{4}e^{-\frac{4x}{3}}. \tag{58}
$$

Then by using (20) and (58), the symbol error probability for the ith hop can be obtained as

$$
\begin{aligned}
\Theta_i^{\mathrm{HD}} &= \int_0^{\infty}p_{i|\gamma_{S_i}}f_{\gamma_{S_i}}(z)\,\mathrm{d}z\simeq\int_0^{\infty}\left(\frac{e^{-x}}{12}+\frac{e^{-\frac{4x}{3}}}{4}\right)\\
&\quad\times\left(\frac{d_{i-1,i}^{\alpha}e^{-\frac{xd_{i-1,i}^{\alpha}}{P_T}-x^{\frac{2}{\alpha}}\Omega_i}}{P_T}+\frac{2\Omega_i x^{\frac{2}{\alpha}-1}}{\alpha}\right)\mathrm{d}x\\
&= \frac{36}{\sqrt{9\frac{d_{i-1,i}^{\alpha}}{P_T}+12}\left(\frac{d_{i-1,i}^{\alpha}}{P_T}+1\right)^{\frac{5}{2}}\left(72\frac{d_{i-1,i}^{\alpha}}{P_T}+96\right)}\\
&\quad\times\left(\Omega_i\sqrt{\pi}\left(\frac{d_{i-1,i}^{\alpha}}{P_T}+1\right)^{\frac{5}{2}}e^{\frac{3\Omega_i^2}{12\frac{d_{i-1,i}^{\alpha}}{P_T}+16}}\operatorname{erfc}\left(\frac{3\Omega_i}{2\sqrt{9\frac{d_{i-1,i}^{\alpha}}{P_T}+12}}\right)\right.\\
&\quad\times\frac{\sqrt{9\frac{d_{i-1,i}^{\alpha}}{P_T}+12}}{12}\left(\left(\frac{d_{i-1,i}^{\alpha}}{P_T}+1\right)\Omega_i\sqrt{\pi}\operatorname{erfc}\left(\frac{\Omega_i}{2\sqrt{\frac{d_{i-1,i}^{\alpha}}{P_T}+1}}\right)\right.\\
&\quad\times\left(\frac{d_{i-1,i}^{\alpha}}{P_T}+\frac{4}{3}\right)e^{\frac{\Omega_i^2}{4\frac{d_{i-1,i}^{\alpha}}{P_T}+4}}-8\left(\frac{d_{i-1,i}^{\alpha}}{P_T}+1\right)^{\frac{3}{2}}\frac{d_{i-1,i}^{\alpha}}{P_T}\\
&\quad\left.\left.\times\left(\frac{d_{i-1,i}^{\alpha}}{P_T}+\frac{13}{12}\right)\right)\right).
\end{aligned}
\tag{59}
$$

REFERENCES

[1] C. T. Cheng, N. Ganganath, and K. Y. Fok, "Concurrent data collection trees for IoT applications," *IEEE Trans. Ind. Informat.*, vol. 13, no. 2, pp. 793–799, Apr. 2017.

[2] S. Chen, H. Xu, D. Liu, B. Hu, and H. Wang, "A vision of IoT: Applications, challenges, and opportunities with China perspective," *IEEE Internet Things J.*, vol. 1, no. 4, pp. 349–359, Aug. 2014.

[3] A. Al-Fuqaha, M. Guizani, M. Mohammadi, M. Aledhari, and M. Ayyash, "Internet of Things: A survey on enabling technologies, protocols, and applications," *IEEE Commun. Surveys Tuts.*, vol. 17, no. 4, pp. 2347–2376, 4th Quart., 2015.

[4] J. Tang, D. K. C. So, N. Zhao, A. Shojaeifard, and K. Wong, "Energy efficiency optimization with swipt in MIMO broadcast channels for Internet of Things," *IEEE Internet Things J.*, vol. 5, no. 4, pp. 2605–2619, Aug. 2018.

[5] H. Nishiyama, M. Ito, and N. Kato, "Relay-by-smartphone: Realizing multihop device-to-device communications," *IEEE Commun. Mag.*, vol. 52, no. 4, pp. 56–65, Apr. 2014.

[6] S. Chen and J. Zhao, "The requirements, challenges, and technologies for 5G of terrestrial mobile telecommunication," *IEEE Commun. Mag.*, vol. 52, no. 5, pp. 36–43, May 2014.

[7] G. Chen, J. Tang, and J. P. Coon, "Optimal routing for multihop social-based D2D communications in the Internet of Things," *IEEE Internet Things J.*, vol. 5, no. 3, pp. 1880–1889, Jun. 2018.

[8] J. Tang, G. Chen, and J. P. Coon, "Route selection based on connectivity-delay-trust in public safety networks," *IEEE Syst. J.*, to be published.

[9] W. Roh *et al.*, "Millimeter-wave beamforming as an enabling technology for 5G cellular communications: Theoretical feasibility and prototype results," *IEEE Commun. Mag.*, vol. 52, no. 2, pp. 106–113, Feb. 2014.

[10] M. Jain *et al.*, "Practical, real-time, full duplex wireless," in *Proc. ACM MobiCom*, Sep. 2011, pp. 301–312.

[11] B. Debaillie *et al.*, "Analog/ RF solutions enabling compact full-duplex radios," *IEEE J. Sel. Areas Commun.*, vol. 32, no. 9, pp. 1662–1673, Oct. 2014.

[12] H. Ju, S. Lim, D. Kim, H. V. Poor, and D. Hong, "Full duplexity in beamforming-based multi-hop relay networks," *IEEE J. Sel. Areas Commun.*, vol. 30, no. 8, pp. 1554–1565, Sep. 2012.

[13] P. Wu, R. Schober, and V. K. Bhargava, "Robust transceiver design for SC-FDE multi-hop full-duplex decode-and-forward relaying systems," *IEEE Trans. Wireless Commun.*, vol. 15, no. 2, pp. 1129–1145, Feb. 2016.

[14] T. K. Baranwal, D. S. Michalopoulos, and R. Schober, "Outage analysis of multihop full duplex relaying," *IEEE Commun. Lett.*, vol. 17, no. 1, pp. 63–66, Jan. 2013.

[15] J. Park, Y. Kim, G. Kim, and H. Lim, "Power allocation for multi-hop transmission using unsaturated full-duplex relay network model," *IEEE Wireless Commun. Lett.*, to be published.

[16] C. Bockelmann *et al.*, "Massive machine-type communications in 5G: Physical and MAC-layer solutions," *IEEE Commun. Mag.*, vol. 54, no. 9, pp. 59–65, Sep. 2016.

[17] M. Haenggi, *Stochastic Geometry for Wireless Networks*. Cambridge, U.K.: Cambridge Univ. Press, 2012.

[18] A. Ghasemi and E. S. Sousa, "Fundamental limits of spectrum-sharing in fading environment," *IEEE Trans. Wireless Commun.*, vol. 6, no. 2, pp. 649–658, Feb. 2007.

[19] K. Hamdi, W. Zhang, and K. B. Letaief, "Power control in cognitive radio systems based on spectrum sensing side information," in *Proc. IEEE Int. Conf. Commun.*, Glasgow, U.K., Jun. 2007, pp. 5161–5165.

[20] M. Hasan, E. Hossain, and D. I. Kim, "Resource allocation under channel uncertainties for relay-aided device-to-device communication underlaying LTE-A cellular networks," *IEEE Trans. Wireless Commun.*, vol. 13, no. 4, pp. 2322–2338, Apr. 2014.

[21] G. Chen, Z. Tian, Y. Gong, Z. Chen, and J. A. Chambers, "Max-ratio relay selection in secure buffer-aided cooperative wireless networks," *IEEE Trans. Inf. Forensics Security*, vol. 9, no. 4, pp. 719–729, Apr. 2014.

[22] G. Chen, Y. Gong, P. Xiao, and J. A. Chambers, "Physical layer network security in the full-duplex relay system," *IEEE Trans. Inf. Forensics Security*, vol. 10, no. 3, pp. 574–583, Apr. 2015.

[23] R. H. Y. Louie, Y. Li, and B. Vucetic, "Practical physical layer network coding for two-way relay channels: Performance analysis and comparison," *IEEE Trans. Wireless Commun.*, vol. 9, no. 2, pp. 764–777, Feb. 2010.

[24] S. Hong *et al.*, "Applications of self-interference cancellation in 5G and beyond," *IEEE Commun. Mag.*, vol. 52, no. 2, pp. 114–121, Feb. 2014.
[25] T. Riihonen, S. Werner, and R. Wichman, "Hybrid full-duplex/half-duplex relaying with transmit power adaptation," *IEEE Trans. Wireless Commun.*, vol. 10, no. 9, pp. 3074–3085, Sep. 2011.
[26] G. Chen, J. P. Coon, and M. D. Renzo, "Secrecy outage analysis for downlink transmissions in the presence of randomly located eavesdroppers," *IEEE Trans. Inf. Forensics Security*, vol. 12, no. 5, pp. 1195–1206, May 2017.
[27] I. S. Gradshteyn and I. M. Ryzhik, *Table of Integrals, Series, and Products*. Waltham, MA, USA: Academic, 2007.
[28] *NIST Digital Library of Mathematical Functions, Release 1.0.19*, F. W. J. Olver *et al.*, Eds., Jun. 2018. [Online]. Available: http://dlmf.nist.gov/
[29] M. Chiani, D. Dardari, and M. K. Simon, "New exponential bounds and approximations for the computation of error probability in fading channels," *IEEE Trans. Wireless Commun.*, vol. 2, no. 4, pp. 840–845, Jul. 2003.

Gaojie Chen (S'09–M'12–SM'18) received the B.Eng. degree in electrical information engineering and the B.Ec. degree in international economics and trade from Northwest University, Xi'an, China, in 2006, and the M.Sc. (Hons.) and Ph.D. degrees in electrical and electronic engineering from Loughborough University, Loughborough, U.K., in 2008 and 2012, respectively.

From 2008 to 2009, he was a Software Engineer with DTmobile, Beijing, China. From 2012 to 2013, he was a Research Associate with the School of Electronic, Electrical and Systems Engineering, Loughborough University. He was a Research Fellow with 5GIC, Faculty of Engineering and Physical Sciences, University of Surrey, Guildford, U.K., from 2014 to 2015. He was a Research Associate with the Department of Engineering Science, University of Oxford, Oxford, U.K., from 2015 to 2018. He is currently a Lecturer with the Department of Engineering, University of Leicester, Leicester, U.K. His current research interests include information theory, wireless communications, cooperative communications, cognitive radio, secrecy communication, and random geometric networks.

Dr. Chen has been serving as an Editor for *IET Electronics Letters* since 2018.

Justin P. Coon (S'02–M'05–SM'10) received the B.Sc. degree (with Distinction) in electrical engineering from the Calhoun Honors College, Clemson University, Clemson, SC, USA, and the Ph.D. degree in communications from the University of Bristol, Bristol, U.K., in 2000 and 2005, respectively.

In 2004, he joined the Bristol-based Telecommunications Research Laboratory (TRL), Toshiba Research Europe Ltd., Cambridge, U.K., as a Research Engineer, where he conducted research on a broad range of communication technologies and theories, including single and multicarrier modulation techniques, estimation and detection, diversity methods, and system performance analysis and networks. He was a Research Manager with TRL from 2010 to 2013, where he led all theoretical and applied research on the physical layer. He was a Visiting Fellow with the School of Mathematics, University of Bristol, from 2010 to 2012, where he was also a Reader with the Department of Electrical and Electronic Engineering from 2012 to 2013. He joined the University of Oxford, Oxford, U.K., in 2013, where he is currently an Associate Professor with the Department of Engineering Science and a Tutorial Fellow of Oriel College. He has authored or co-authored publications in excess of 150 papers in leading international journals and conferences, and is a named inventor on over 30 patents. His current research interests include communication theory, information theory, and network theory.

Dr. Coon was a recipient of the TRL's Distinguished Research Award for his research on block-spread CDMA, aspects of which have been adopted as mandatory features in the 3GPP LTE Rel-8 Standard. He was also a co-recipient of Two Best Paper Awards for work presented at ISWCS 13 and EuCNC 14. He served as an Editor for the IEEE TRANSACTIONS ON WIRELESS COMMUNICATIONS from 2007 to 2013 and the IEEE TRANSACTIONS ON VEHICULAR TECHNOLOGY from 2013 to 2016. He has been serving as an Editor for the IEEE WIRELESS COMMUNICATIONS LETTERS since 2016 and the IEEE COMMUNICATIONS LETTERS since 2017.

Avishek Mondal is currently pursuing the undergraduation degree with the Department of Engineering Science, University of Oxford, Oxford, U.K.

He is currently a Visiting Student with the Department of Electrical Engineering, Princeton University, Princeton, NJ, USA.

Ben Allen (M'04–SM'05) is a Royal Society Industry Fellow with the University of Oxford, Oxford, U.K., and Network Rail, London, U.K., where he is an accomplished and experienced Research Engineer in the field of telecommunications, and is currently researching innovative means of improving the digital connectivity of railways and passengers. He has authored around 150 technical papers and 3 books.

Mr. Allen is an Associate Editor of the *Proceedings of the Royal Society A: Mathematical, Physical and Engineering Sciences* and a past Associate Editor of *IET Microwaves, Antennas and Propagation*. He is a Fellow of the IET and a Chartered Engineer.

Jonathon A. Chambers (S'83–M'90–SM'98–F'11) received the D.Sc. and Ph.D. degrees in signal processing from Imperial College London, London, U.K., in 1990 and 2014, respectively.

From 1991 to 1994, he was a Research Scientist with the Schlumberger Cambridge Research Center, Cambridge, U.K. In 1994, he returned to Imperial College London, as a Lecturer in signal processing and became a Reader (Associate Professor) in 1998. From 2001 to 2004, he was the Director of the Center for Digital Signal Processing and a Professor of signal processing with the Division of Engineering, King's College London, London, where he is currently a Visiting Professor. From 2004 to 2007, he was a Cardiff Professorial Research Fellow with the School of Engineering, Cardiff University, Cardiff, U.K. From 2007 to 2014, he led the Advanced Signal Processing Group, School of Electronic, Electrical and Systems Engineering, Loughborough University, Loughborough, U.K., where he is also a Visiting Professor. In 2015, he joined the School of Electrical and Electronic Engineering, and he has been with the School of Engineering, Newcastle University, Newcastle upon Tyne, U.K., since 2017. Since 2017, he has also been a Professor of engineering and the Head of Department with the University of Leicester, Leicester, U.K. He is also the International Honorary Dean and a Guest Professor with the Department of Automation, Harbin Engineering University, Harbin, China. He has advised almost 80 researchers through to Ph.D. graduation and has published over 500 conference proceedings and journal articles, many of which are in IEEE journals. His current research interests include adaptive signal processing and machine learning and their applications in communications, defense, and navigation systems.

Dr. Chambers was a Technical Program Co-Chair of the 36th IEEE International Conference on Acoustics, Speech, and Signal Processing (ICASSP), Prague, Czech Republic. He is serving on the Organizing Committees of ICASSP 2019, Brighton, U.K., and ICASSP 2022, Singapore. He has served on the IEEE Signal Processing Theory and Methods Technical Committee for six years, the IEEE Signal Processing Society Awards Board for three years, and the Jack Kilby Medal Committee for three years. He was an Associate Editor of the IEEE TRANSACTIONS ON SIGNAL PROCESSING from 1997 to 1999 and from 2004 to 2007, and a Senior Area Editor from 2011 to 2015. He is a Fellow of the Royal Academy of Engineering, London, the Institution of Engineering and Technology, and the Institute of Mathematics and its Applications.